JMEPEG
https://doi.org/10.1007/s11665-024-10079-4

1059-9495/$19.00

ORIGINAL RESEARCH ARTICLE

Effect of Heat Treatment on Microstructure and Mechanical Properties of a New Alpha-Titanium Alloy Ti-6.0Al-3.0Zr-0.5Sn-1.0Mo-1.5Nb-1.0V

Yongsheng Wang, Meiyu Hou, Zhirong Huang, Yaoping Xu, Cong Tan, and Han Xiao

Submitted: 10 July 2023 / Revised: 19 May 2024 / Accepted: 7 July 2024

A new α-titanium alloy Ti-6.0Al-3.0Zr-0.5Sn-1.0Mo-1.5Nb-1.0 V (Ti603) with high strength was investigated. The ingot was initially hot rolled into sheet. Then the sheet was annealed at 740 °C for 1 h; meanwhile, it was subjected to solution treatment at 900 °C for 0.5 h, followed by aging treatment at 580 °C for 3 h. The microstructure and texture of the alloy were characterized by electron backscatter diffraction (EBSD). The results show that the microstructure of the alloy evolved from lamellar to equiaxed after annealing and solid solution aging treatment. In addition, the grain size of the solid solution aging treated sample was larger compared to the annealed sample. After annealing, low-angle grain boundaries (LAGBs) are transformed into high-angle grain boundaries (HAGBs) due to the occurrence of dynamic recrystallization (DRX). This weakened the dislocations accumulation and entanglement at the grain boundaries, resulting in change in grain orientation, thereby reducing the texture strength of the sample. After solution and aging treatment, the stress concentration at the grain boundary increases, and the preferred orientation of the grains changes, resulting in a slight increase in the texture strength of the sample.

Keywords crystal texture, heat treatment, mechanical properties, microstructure evolution, titanium alloy

1. Introduction

With high specific strength and corrosion resistance, titanium alloys are widely used in marine engineering equipment, advanced ship equipment and other fields (Ref 1, 2). High-strength corrosion-resistant titanium alloys generally require titanium alloys with strength above 800 MPa and good corrosion resistance (Ref 3). Although titanium alloys have excellent corrosion resistance and good heat resistance, the current marine titanium alloys have the disadvantages of low strength, insufficient rigidity and large rebound of the alloy during cold forming (Ref 4). Therefore, there is an urgent need to develop new titanium alloys with high-strength and good corrosion resistance to be in line with the international landscape and domestic marine strategies. The traditional high-strength titanium alloy refers to the titanium alloy whose room temperature tensile strength is higher than that of 1100 MPa after heat treatment, while the high-strength corrosion-resistant titanium alloy requires the strength of titanium alloy to be above 800 MPa, which belongs to medium strength titanium alloy (Ref 5). At present, the most successful titanium alloy with high-strength and corrosion resistance is Ti80 (Ti-6Al-3Nb-2Zr-1Mo) titanium alloy (Ref 6). In addition, metastable near β-type TB6 titanium alloy exhibits higher tensile strength of over 1000 MPa and excellent corrosion resistance, making it a popular choice in various applications (Ref 7, 8).

Al is the most important α-stabilizing element in Ti, which can form a substitutional solid solution with Ti and improve the strength and heat resistance of Ti. Elements Mo and Nb, which are widely used in titanium alloys, experience infinite solid solution in the beta phase and stabilize it, which improves the strength of the alloys without lessening their good plasticity (Ref 9). Zr and Sn, two neutral elements with high solubility in both α-Ti and β-Ti, are often used as solid solution elements, which make alloys more workable by lowering their elastic modulus (Ref 10). Meng et al. (Ref 11) studied the corrosion behavior of a Ti-6Al-3Nb-2Zr-1Mo (Ti80) titanium alloy at different annealing temperatures. The results showed that the passivation film formed by Zr, Nb and Mo oxides in the titanium alloy was denser than that formed by Al, which significantly improved the corrosion resistance of the alloy.

Heat treatment is a common way to improve the strength, plasticity and corrosion resistance of titanium alloys during

Yongsheng Wang, Meiyu Hou, and **Zhirong Huang**, Faculty of Materials Science and Engineering, Kunming University of Science and Technology, Kunming 650093, China; National-Local Joint Engineering Laboratory for Technology of Advanced Metallic Solidification Forming and Equipment, Kunming University of Science and Technology, Kunming 650093, China; and Yunnan Titanium Industry Co. Ltd, Chuxiong 651209 Yunnan, China; **Yaoping Xu**, Yunnan Titanium Industry Co. Ltd, Chuxiong 651209 Yunnan, China; and **Cong Tan** and **Han Xiao**, Faculty of Materials Science and Engineering, Kunming University of Science and Technology, Kunming 650093, China; and National-Local Joint Engineering Laboratory for Technology of Advanced Metallic Solidification Forming and Equipment, Kunming University of Science and Technology, Kunming 650093, China. Contact e-mail: kmxh@kust.edu.cn.

Published online: 16 September 2024

their preparation. In this way, titanium alloys with excellent comprehensive properties can be produced by constantly changing the microstructure (Ref 12). Tsai et al. (Ref 13) investigated the effect of heat treatment on the microstructure and properties of 3D-printed TC4 titanium alloys at temperatures between 550 °C and 800 °C. The results showed that after the annealing at 600 °C, residual stresses were eliminated; the $\alpha' \rightarrow \alpha+\beta$ phase transformation happened in the microstructure; dislocations and twinning were gone, and the alloys presented lower tensile strength and higher elongation. Davari et al. (Ref 14) studied the microstructure and mechanical properties of TC4 titanium alloys annealed at 930 °C and 970 °C. The results showed that as the annealing temperature rose, the aspect ratio and volume fraction of the primary α phase decreased significantly while the content of the residual β phase increased drastically, resulting in higher hardness and tensile strength. After solution treatment, the supersaturated solid solution was obtained during the rapid cooling process, and the β phase was transformed into martensitic α phase or metastable β phase. But the transformation brings slight lattice deformation and the strengthening effect is not significant. After aging treatment, the martensite phase will decompose into a fine secondary alpha phase, which diffuses in the beta phase so that aging treatment can play its role (Ref 15, 16). Li et al. (Ref 17) investigated the effects of different solution temperatures on the microstructure and properties of a Ti-6Cr-5Mo-5 V-4Al titanium alloy. The results showed that the primary α phase formed during the α/β solution treatment of the alloy could increase the stability of the β matrix and inhibit the growth of the secondary α phase in the aging process. The β matrix became unstable after β solution treatment. The driving force of the second phase was larger, so the coarser α phase was formed and unevenly distributed in the aging process, resulting in lower strength and elongation. Solution temperatures can also influence the content of the metastable phase produced by solid solution treatment of the titanium alloy, which dampens the role of aging treatment. The effect of solution treatment on the microstructure and mechanical properties of a new TG6 titanium alloy has been systematically analyzed by Yu et al. (Ref 18). But the results showed that solution temperature mainly affected the content of the α phase. When the temperature range was 850-1050 °C, the content of the primary α phase decreased with the solution temperature, while the secondary α phase experienced a lamellar-to-acicular transformation as the temperature became increasingly higher. These previous studies have shown that the mechanical properties of titanium alloys can be optimized by heat treatment schedule regulation. Reasonable heat treatment of hot-rolled titanium alloy sheets can prolong the service life, eliminate residual stress and remove work hardening. The heat treatment processes have a significant effect on the microstructures and properties of marine near-α titanium alloys; the change of heat treatment parameters can affect the morphology, size and volume fraction of α phase, β phase and secondary α phase. Solid solution and aging are the main heat treatment strengthening methods of titanium alloy. The metastable phase is formed during the cooling process after solid solution, and the secondary α phase is precipitated by the decomposition of the metastable phase during the later aging process. Combined with the change of the distribution and volume fraction of the equiaxed primary α phase, the purpose of strengthening and toughening is achieved.

In the previous work, we studied the effect of annealing time on the microstructure and mechanical properties of Ti-6.0Al-3.0Zr-0.5Sn-1.0Mo-1.5Nb-1.0 V (Ti603) titanium alloy, and obtained a better annealing time range (Ref 19). In this study, based on the previous work, the effects of different heat treatment processes on the microstructure and mechanical properties of the new titanium alloy were studied. The EBSD characterization method was used to analyze the reasons why different heat treatment methods affect the microstructure and properties of the titanium alloy. It provides theoretical basis and guidance for heat treatment process of high-strength corrosion-resistant titanium alloy.

2. Materials and Experimental Procedures

A Ti-6.0Al-3.0Zr-0.5Sn-1.0Mo-1.5Nb-1.0 V (Ti603) alloy ingot was produced. It was melted three times in a VAR furnace, which was made by Yunnan Titanium Industry Co., Ltd. The alloy ingots are processed into plates by forging and hot rolling. The chemical composition (wt.%) of the as-cast Ti603 is shown in Table 1. The $\alpha+\beta/\beta$ phase transition temperature of Ti603 titanium alloy calculated by Pandat software is 967.92 °C, as shown in Fig. 1. The hot rolling (HR) process is shown in Table 2. The hot-rolled sheets were annealed at 740 °C/1 h (HT1), 900 °C/0.5 h solution treatment and 580 °C/3 h aging treatment (HT2). Figure 2 illustrates how hot rolling, heat treatment and microstructure observation were done. Before the heat treatment, the Ti603 alloy was covered with an antioxidant coating to avoid oxidation during the

Table 1 Chemical composition of the as-cast Ti603 (wt.%)

Ti	Al	Zr	Sn	Mo	Nb	V	C	O
Bal.	5.93	2.99	0.58	0.91	1.34	0.87	0.017	0.084

Table 2 Hot rolling process of the Ti603 alloy

No.	Initial thickness, mm	Target thickness, mm	Total reduction, mm	Total reduction rate, %	Rolling temperature, °C
1	110	35	75	68.2	960
2	35	15	20	57.1	950
3	15	8	7	46.7	940

heating process. The antioxidant coating was removed, and the alloy's surface was polished after heat treatment.

The tensile test was carried out by MTS model E45 microcomputer control servo universal room temperature tensile testing machine. Before the single room temperature stretching, the tensile specimen is polished to smooth and non-oxidized skin by using 200 mesh and 400 mesh sandpaper from small to large, and the stretching speed is 5 mm/min. Each group of samples is tested three times, and the results are averaged to ensure the authenticity and reliability of the test results. The hot-rolled and heat-treated Ti603 sheet was cut into metallographic samples of 10*10*8 mm by using wire electrical discharge machining (WEDM). Then they were polished with sandpapers and etched in Koll reagent, which had the volume ratio of HF: HNO_3: H_2O=1:2:7. Their microstructures were observed by a Nikon Eclipse MA200 optical microscope (OM). The microstructures of these samples were observed from the RD-TD plane. The phases of the alloy were analyzed through x-ray diffraction (XRD) patterns with Cu target and Kα radiation source. The scanning rate was 10°/min. To conduct the EBSD observation, the samples were ground with silicon carbide (SiC) grit papers ranging from 120 to 1000#, and electro-polished (voltage: 17 V) in solution with 60% methanol, 34% n-butyl alcohol and 6% perchloric acid at room temperature to remove the stress layer. They were examined by a HitachiS-3400 N scanning electron microscope equipped with an EBSD system. The scanning step is 0.3 μm, and the scanning area is 350 μm × 250 μm. HKL Technology Channel 5 was used to analyze data, including grain sizes, grain boundaries, orientation and recrystallization fraction.

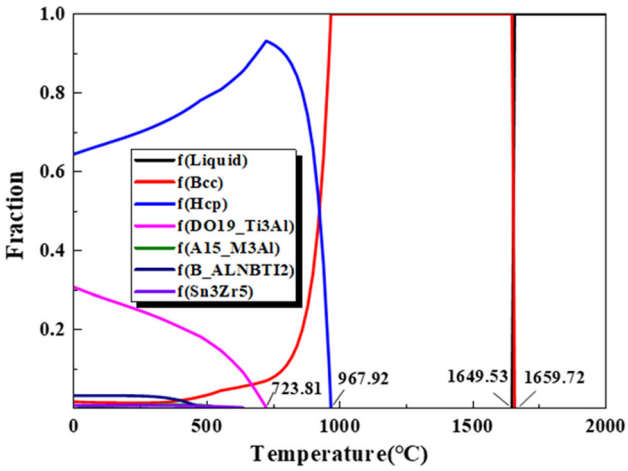

Fig. 1 Phase transformation diagram of Ti603 alloy (Color figure online)

3. Results and Discussion

3.1 Microstructure Characterization

The surface scanning energy spectrum of the cross section of hot-rolled sheets is shown in Fig. 3. Studies (Ref 11, 20) suggested that the Al in titanium alloys could stabilize the α-phase and that its solid solubility in the α-phase was higher than that in the β-phase. While elements Nb, Mo and can stabilize the β-phase, and it enjoys better solid solubility in the β-phase than in the α-phase. The energy spectrum, however, shows that the element distribution was relatively uniform. Elements showed an insignificant difference in terms of solid solution in the α phase and the β phase, which may be explained by the low content of Mo, Nb and in the alloy.

3.2 Microstructure Evolution and Phases Analysis After Heat Treatment

Figure 4 shows the XRD patterns of the alloy after different heat treatments. It is dominated by α-Ti (PDF#44-1294) and β-Ti (PDF#44-1288) phases (Ref 21, 22). The highest peak occurred at around 2θ=38.4° under different heat treatments. The sheet annealed at 740 °C exhibited a significantly stronger

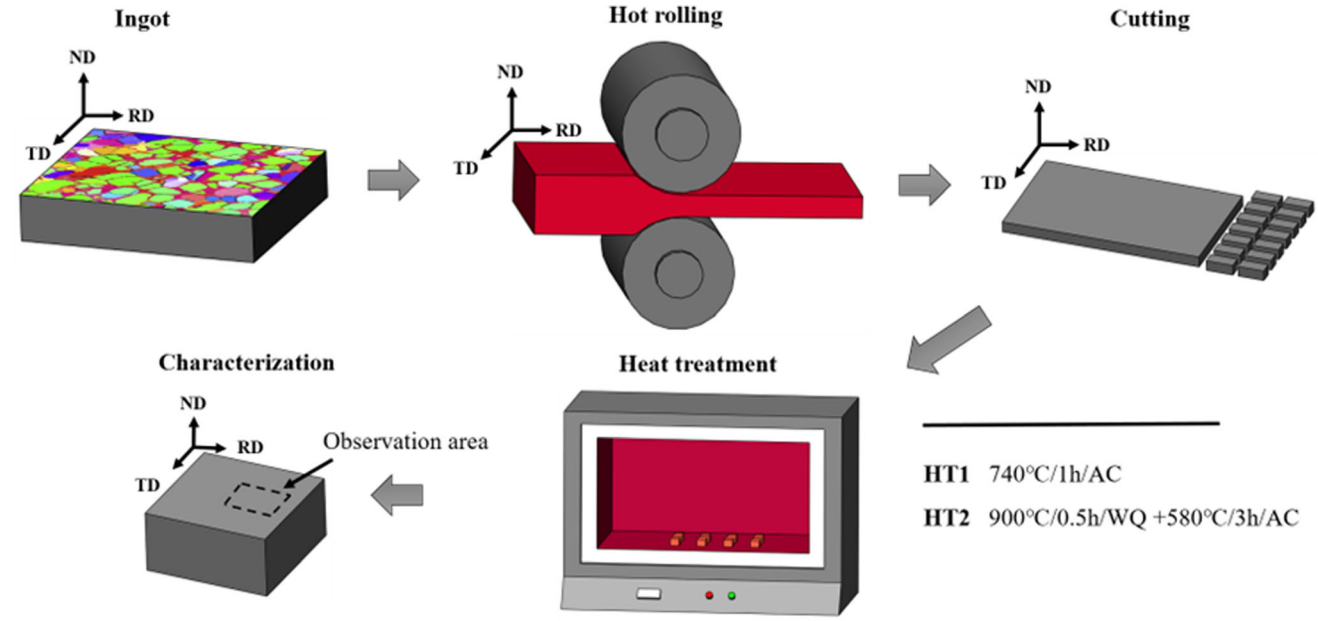

Fig. 2 Experimental procedure (hot rolling, annealing and microstructure observation)

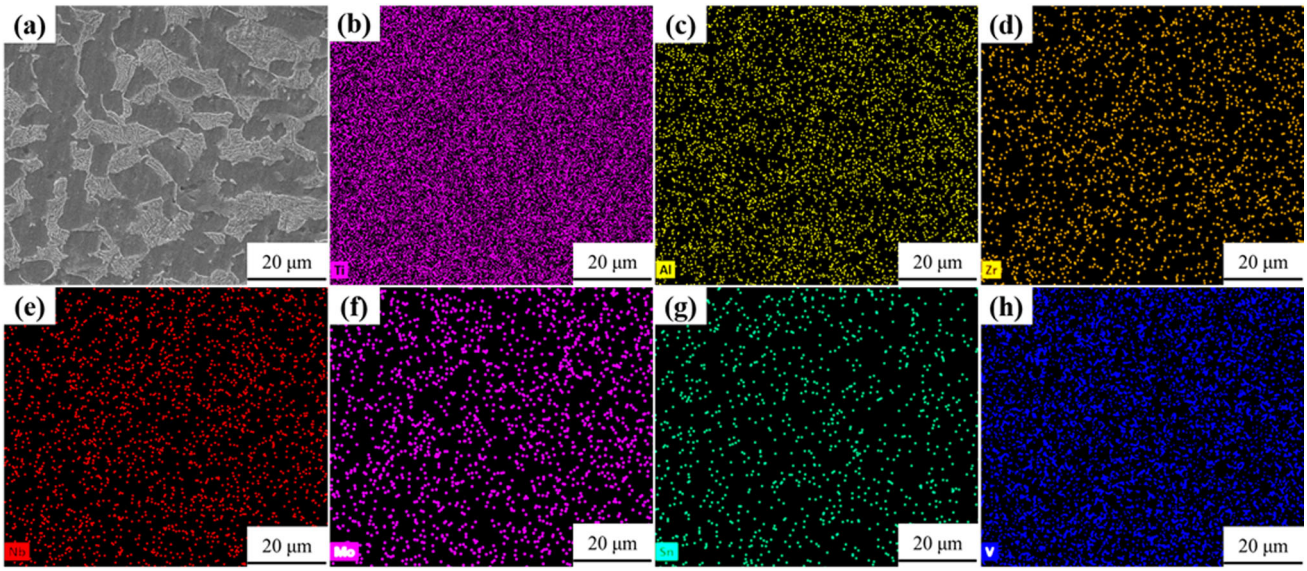

Fig. 3 Surface scanning energy spectrum of (a) the surface and elements (b) Ti, (c) Al, (d) Zr, (e) Nb, (f) Mo, (g) Sn and (h) V of the alloy (Color figure online)

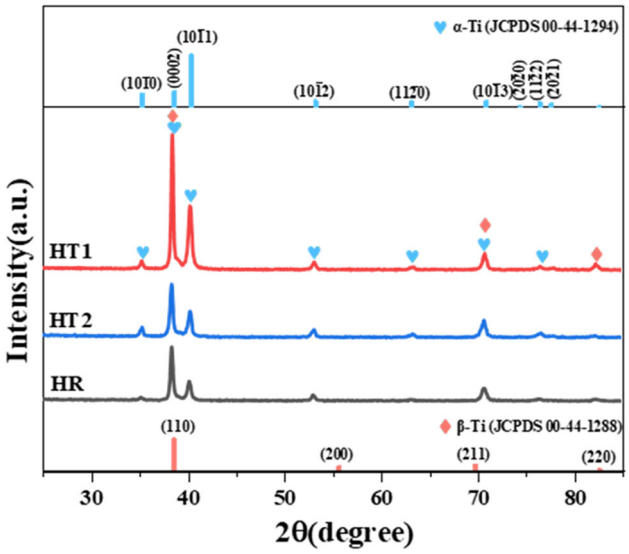

Fig. 4 XRD patterns of Ti603 titanium alloy (Color figure online)

α-phase diffraction peak than the hot-rolled (0002) one, which was because of the sufficient holding time after annealing, enabling grains to fully grow. After solution treatment at 900 °C and aging treatment at 580 °C, the diffraction peak intensity of α phase (0002) of the sample is not much different from that of the hot-rolled sample. The (0002) α and (10-10) α diffraction peaks were located at 38.42° and 40.17° in the standard PDF card of α-Ti. In the x-ray patterns of the annealed alloy receiving solution plus aging treatments, as shown in Fig.4, the alpha diffraction peaks of (0002) occurred at 38.43° and 38.38°, respectively, while those of (10-10) were at 40.27° and 40.30°, with a slight of deviation. This indicated that other elements had an insignificant effect on the lattice constant of the alloy after heat treatment (Ref 18, 23).

The microstructure of the HR Ti603 alloy is shown in Fig. 5 (a). The β phase is located in the grayish-black area, and the α phase in the grayish-white area. The microstructure of the hot-rolled alloy is dominated by the elongated primary α phase (α_p) and the β transformation structure. Both α and β phases elongated along the rolling direction. During hot rolling, the $\alpha \rightarrow \beta$ phase transformation happened when it reached the β phase transition temperature, which enabled the thin and distorted lamellar structure to experience transformation (Ref 24). The β phase was transformed into the secondary α phase in the subsequent air-cooling process. The inverse pole figure (IPF) in Fig. 5(b) shows that the directions of most grains were <0001>and<2-1-10>and that of a small amount of them was< 10-10>. Channel 5 shows that their average grain size was 3.11 μm. The microstructure and grain sizes of the Ti603 alloy annealed at 740 °C are shown in Fig. 5(d), (e) and (f). After annealing, its microstructure became equiaxed and was composed of the α phase and the β transformation structure. The formation of equiaxed grains was a result of adequate recrystallization of grains because of adequate holding time for annealing. Thus the grains were completely recrystallized (Ref 25), and the average grain size was 2.06 μm, which was smaller than that of the hot-rolled alloy. Figure 5(e) presents the orientation distribution of grains in the Ti603 alloy after annealing at 740 °C. The directions are uniform, and grains in directions between<0001>and<2-1-10>turned to between< 0001>and<10-10>. Figure 5(g) shows the microstructure of the alloy receiving solid solution treatment at 900 °C and aging treatment at 580 °C. After solution plus aging treatments, its microstructure was similar to that of the annealed sheet, which was composed of the equiaxed α phase and β transformation structure. The average grain size was 2.30 μm, which was also smaller than that of the hot-rolled alloy. The IPF shows that the number of grains in<2-1-10>direction significantly increased while that in the<0001>direction decreased after solid solution at 900 °C and aging at 580 °C.

3.3 Mechanical Properties

The mechanical properties of Ti603 titanium alloy hot-rolled sheet after different heat treatment are shown in Fig. 6. Figure 6

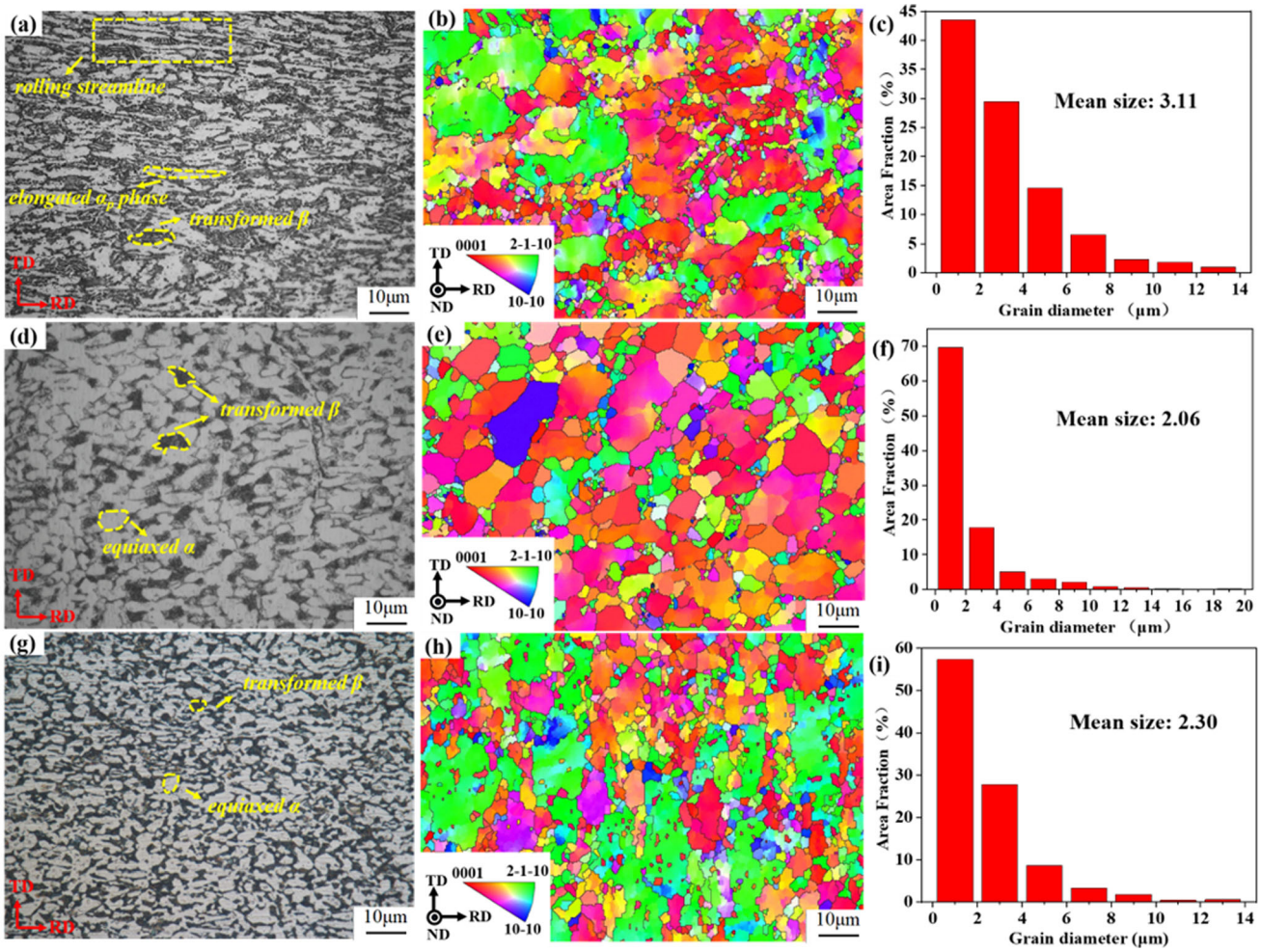

Fig. 5 OM, IPF and grain size distribution of (a, b, c) HR, (d, e, f) HT1 and (g, h, i) HT2 (Color figure online)

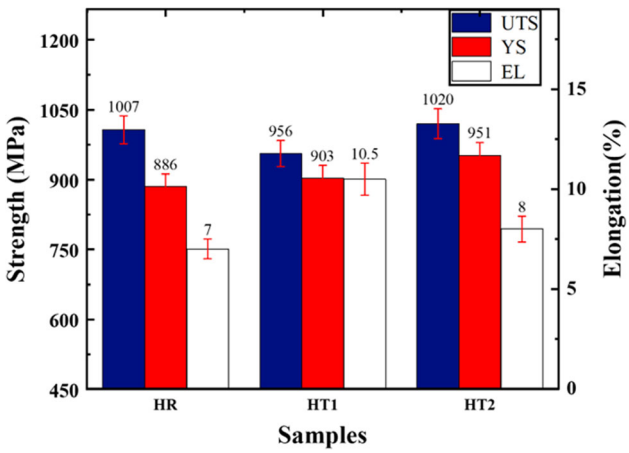

Fig. 6 Mechanical properties of Ti603 titanium alloy with different heat treatment (Color figure online)

shows that the tensile strength of Ti603 titanium alloy hot-rolled sheet is 1007 MPa, and the elongation is 7%. After annealed at 740 °C for 1 h, the strength decreases to 956 MPa, and the elongation increases to 10.5%. The main reason is that after annealing heat treatment, due to recrystallization, equiaxed grains increase, and grains grow obviously. When subjected to continuous external force, large grains first occur intragranular deformation, resulting in the decrease of material strength and the increase of plasticity. After solution aging at 900 °C, the strength is increased to 1020 MPa, and the elongation is 8%. The reason for the improvement of the properties of Ti603 titanium alloy after solution aging is that the microstructure uniformity is improved after solution aging. At the same time, although Ti603 is a near α titanium alloy, there is a part of metastable β phase (β') after solid solution at 900 °C, and the decomposition of $\beta' \rightarrow \alpha_s + \beta$ occurs after aging at 580 °C, resulting in dispersion strengthening effect and improving the strength of the alloy.

Figure 7 shows the tensile fracture morphology of Ti603 titanium alloy under different heat treatment conditions at room temperature. The fracture morphology of the hot-rolled alloy and the alloy after HT1 and HT2 heat treatment has tearing edges and dimples, both of which are ductile fractures. The metal material produces micro-voids in the process of stretching. After continuous external force deformation, the micro-voids grow and nucleate, and then aggregate and fracture to form dimples. Figure 7(a) shows that there are some tearing edges and holes in the fracture morphology of hot-rolled plate in addition to dimples. After annealing at 740 °C, the size of the

dimple is quite uniform, indicating that the plasticity is the best. After HT2 heat treatment, the fracture morphology of the alloy tensile specimen is composed of uneven dimples. The dimples are deeper, and the larger dimples contain a few small dimples, and the plasticity is better.

3.4 Crystal Texture Evolution

The crystal texture of the alloy is formed in thermal mechanical processing (TMP), and heat treatment plays a role in deciding the texture type and intensity of the alloy sheets (Ref 26). The texture composition can be illustrated by PF and orientation distribution function (ODF). Figure 8 shows the typical texture position ($\varphi2=0°$) of the HCP structure (α-Ti) in an ODF diagram (Ref 26, 27), and the grain orientation can be identified in the corresponding position. Under three different heat treatments, ODF diagrams at $\varphi2=0°$ and $\varphi2=30°$ are extracted to accurately characterize texture orientation. As shown in Fig. 9, the HCP structure (α-Ti) and deformed texture can be found on both sections of $\varphi2°=0°$ and $\varphi2°=30°$, which has been confirmed by Wagner et al. (Ref 28). The textures of hot-rolled sheet and heat-treated sheet with HT1 and HT2 are composed of Y-fiber and B-fiber. The texture composition of the original hot-rolled sheet was composed of strong Y-fiber, which is caused by pyramidal<a>slip during rolling. The grain orientation was (11-26)<0-261>, with a strength of 13.3. After annealing at 740 °C, the texture intensity decreased to 8.08, and the corresponding preferred8.08, and the corresponding preferred orientation turned to (03-31)<4-261>, while grain orientation changed to (03-31)<1-139>after solution plus aging treatment. The strength was enhanced to 16.5. After HT1 and HT2 heat treatment, the texture type changed from Y-fiber to dominated by B-fiber. The main reason is that the basal slip is dominant due to the thermal activation during the heat treatment (Ref 29).

3.5 Recrystallization Behavior Analysis

In Channel 5, the determination angle θ of sub-grain boundaries was set at 5°, and that of grain boundaries were at 15°. Under the condition of $5°<\theta$ (angular orientation difference)<15°, grain boundaries are identified as low-angle grain boundaries (LAGBs), see the red line in Fig. 10(a), (b) and (c). But under the condition of $\theta>15°$, they are called high-angle

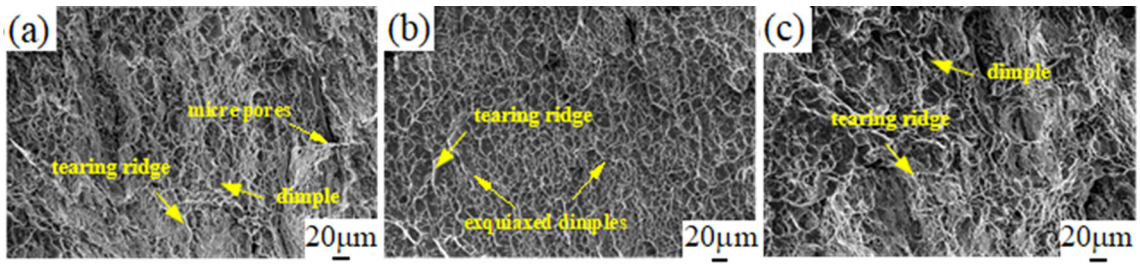

Fig. 7 Tensile fracture of Ti603 titanium alloy at different heat treatment: (a) HR, (b) HT1 and (c) HT2

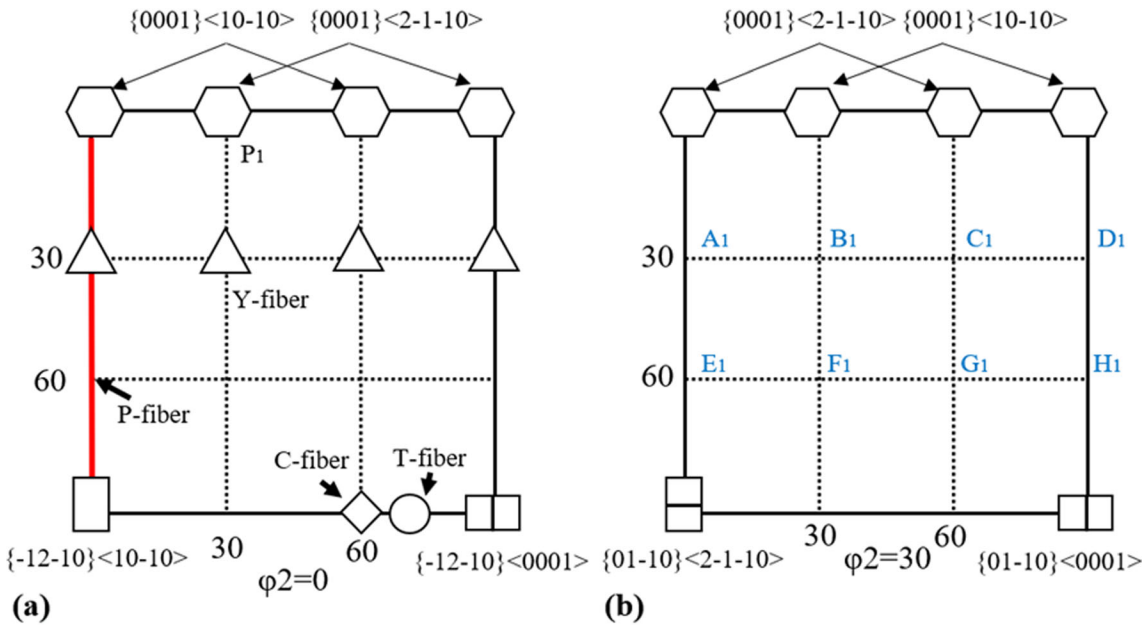

Fig. 8 Typical texture position of HCP structure in ODF: (a) $\varphi2=0°$; (b) $\varphi2=30°$

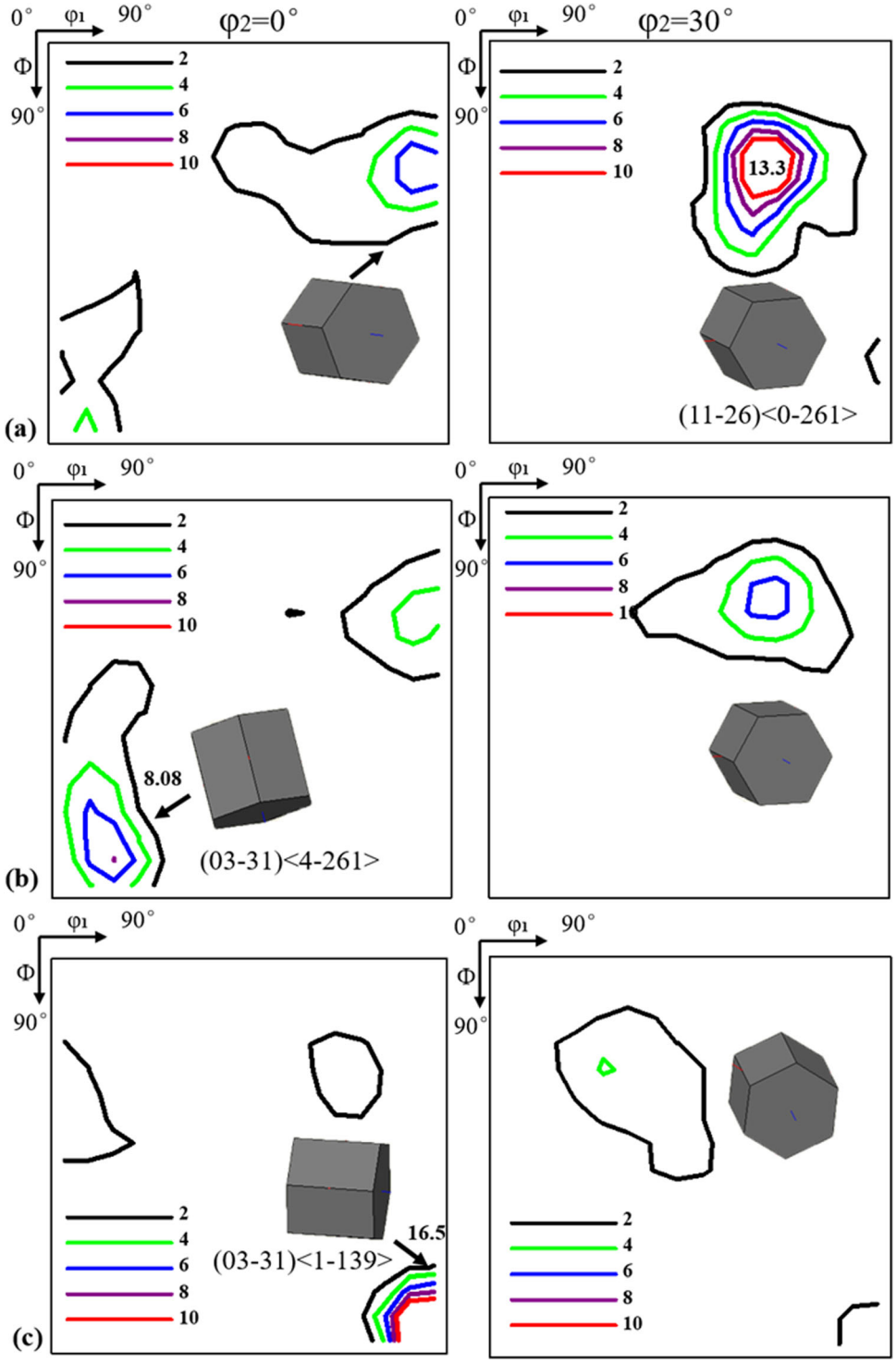

Fig. 9 Texture components displayed in ODF with $\varphi 2°=0°$ and $\varphi 2°=30°$section: (a) HR (b) HT1 (c) HT2 (Color figure online)

grain boundaries (HAGBs), see the black line in Fig. 10(a), (b) and (c) (Ref 30). The hot-rolled alloy is mainly composed of LAGBs, which account for 63.2%. After annealing, however, the number of LAGBs dropped drastically, only accounting for 36.6%, leading to a greater angle. This was caused by recrystallization happening during annealing at 740 °C. In addition, some sub-grains and LAGBs were gradually transformed into new grains to form HAGBs (Ref 31, 32). Two obvious peaks appeared near 60°and 90°after the annealing. According to the Burgers orientation relationship and crystallographic symmetry between the α phase and the β phase in titanium alloys, one β grain may have 12 types of α phase variants, in which there are 5 α/α grain boundaries, as shown in Table 3 (Ref 26, 33). It can be inferred that titanium alloy variants had been selected after annealing. The microstructure of the alloy phases shows that many secondary α phases had

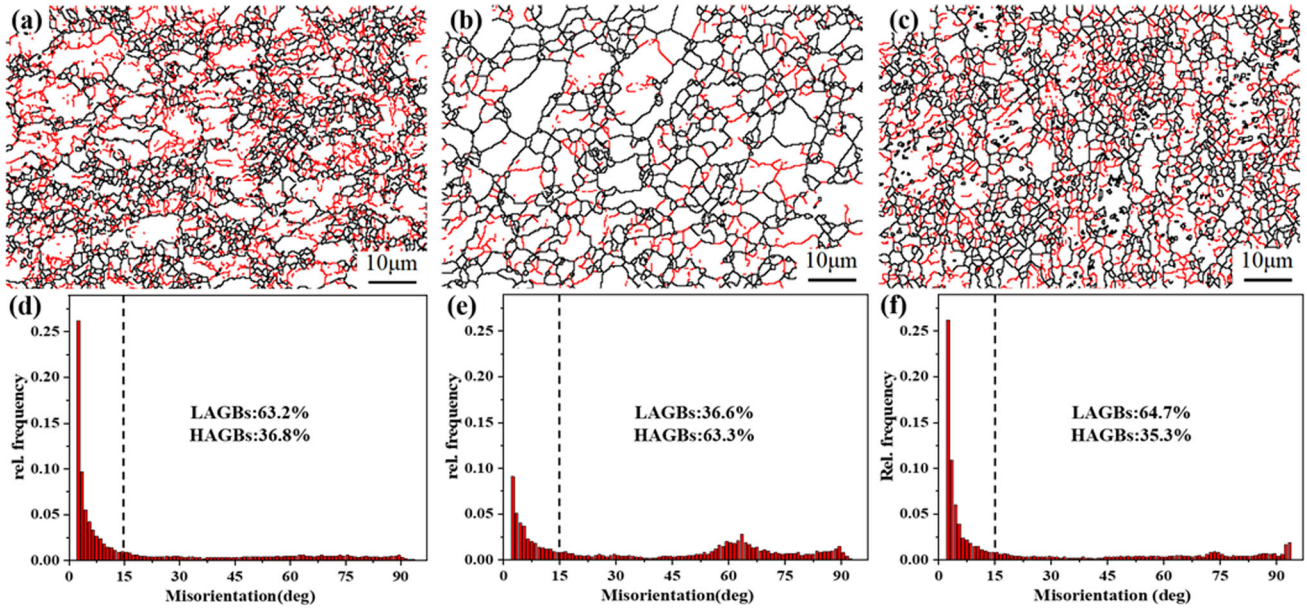

Fig. 10 Grain boundary maps of different Ti603 alloy sheets: (a, d) HR, (b, e) HT1 and (c, f) HT2 (Color figure online)

Table 3 Differences in grain boundary angles of the five types of α/α variants

No	Misorientation angle	Axis
1	10.53	[0 0 0 1]
2	60.00	[1 1−2 0]
3	60.83	[−10−7 17 3]
4	63.26	[−10 5 5 3]
5	90.00	[7−17 10 0]

precipitated on both sides of grain boundaries. After solution plus aging treatments, the angle of grain boundaries and the hot-rolled sheet changed insignificantly, and the sheet was dominated by LAGBs, which accounted for 64.7%.

Titanium alloys will cause dislocation movement (climbing or slipping) within grains during heat treatment, and continuous strain between grains can be realized through the coordination of dislocation density in different areas (Ref 34). The local strain distribution of grains under different heat treatments was analyzed through Ti603 Kernel Average Misorientation (KAM). The results are shown in Fig. 11. The red area is identified as the high-density dislocation area caused by large deformation, while the blue one is the low-density dislocation area caused by small deformation. From the KAM diagram, most of the hot-rolled sheet is found to be yellowish-green, indicating that the strain is more concentrated, which accords with the characteristics of hot rolling. The existence of high strain is partly a result of the slip and entanglement of dislocations happening during hot rolling plastic deformation, and partly because of the phase transformation strain caused by the precipitation of the α phase from the β matrix (Ref 26). After the annealing, the size of the yellow area in the sheet was obviously smaller. The sheet was dominated by the blue area which was distributed on the α phase matrix. Slight strain concentration occurred at grain boundaries, indicating that the disappearance and rearrangement of dislocations were caused by the recrystallization of the alloy after annealing (Ref 35). The red area in the microstructure of the sample receiving solid solution at 900 °C and aging at 580 °C is obviously bigger than that of the hot-rolled one. Most of the grains looked fine, indicating that grains suffered severe lattice distortion after the solid solution, which led to strain concentration in this area.

Figure 12 shows the recrystallization diagrams of Ti603 alloy sheets receiving different heat treatments. In Channel 5, the average orientation difference of grains is represented by the value of the internal average misorientation angle (IAMA). Grains whose IAMA is higher than 1° are identified as deformed (see the red part). If grains contain sub-grains, whose IAMA value is lower than 1°, and the orientation difference between sub-grains is higher than 1°, then these grains have a substructure caused by DRV, which is marked yellow. Other grains are identified as having a recrystallized structure, which is marked in blue (Ref 36). The hot-rolled sheet is mainly composed of a recovery structure, and there is a small amount of recrystallization structure (5.28%), as shown in Fig.12. Much recrystallization structure was found in the sheet annealed at 740 °C, reaching 49.98%. The microstructure of the alloy after solution and aging treatment is mainly composed of recovery substructure and deformed grains, accounting for 65% and 30.04%, respectively. Due to the high temperature of hot rolling, recrystallization happened, but it was incomplete and mainly caused by recovery structure due to the short hot rolling process. During annealing, discontinuous dynamic recrystallization (DDRX) occurred because of air cooling in the $\alpha+\beta$-phase area and sufficient holding time (Ref 37). In the process of DDRX, grains were nucleated through the bow of grain boundaries and rotated with the bow. The nucleation and growth of recrystallized grains consume surrounding disloca-

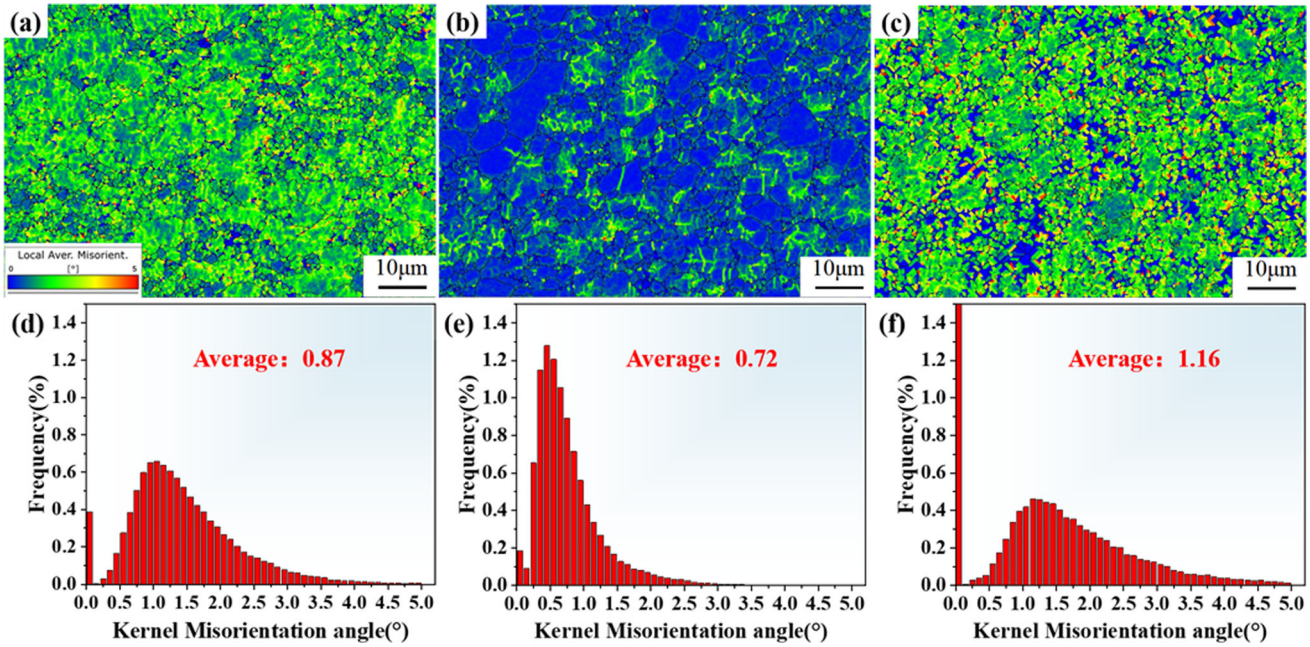

Fig. 11 KAM diagrams of different Ti603 alloy sheets: (a, d) HR, (b, e) HT1 and (c, f) HT2 (Color figure online)

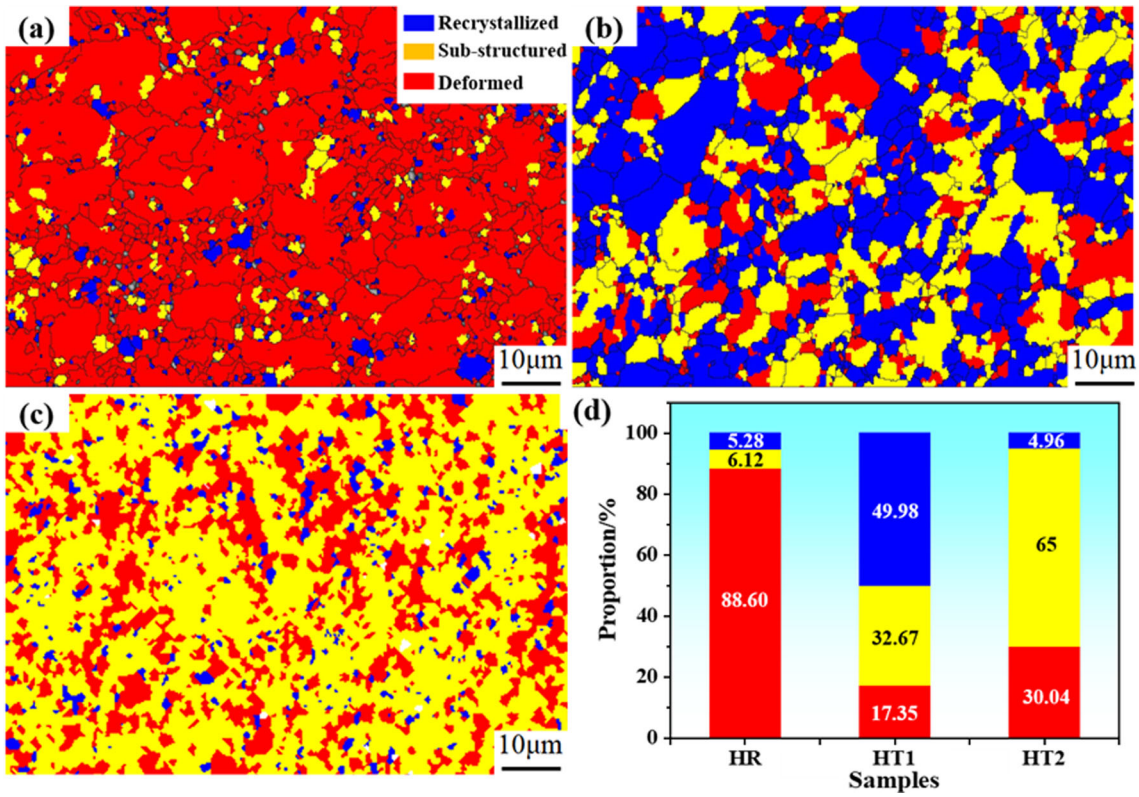

Fig. 12 Recrystallization diagrams of different Ti603 alloy sheets: (a) HR, (b) HT1, (c) HT2 and (d) the proportion of recrystallization, sub-structure and deformation (Color figure online)

tions as the stacking fault energy of β-Ti was low, which was in line with the KAM diagram.

4. Conclusions

This study focused on the effects of different heat treatments on the microstructure and texture of a new type of α titanium alloy Ti-6.0Al-3.0Zr-0.5Sn-1.0Mo-1.5Nb-1.0 V(Ti603) with high strength. The major findings are as follows:

(1) The hot-rolled sheet exhibited deformed lamellar structure, and the grains were elongated along the rolling direction. In addition, some β-transformed structures were observed. After annealing at 740 °C, solution treatment at 900 °C and aging treatment at 580 °C, the microstructure of the sample was equiaxed. The grain size of the sample after solution aging treatment was slightly larger than that after annealing treatment.
(2) The tensile strength of hot-rolled sheet was 1007 MPa, and the elongation was 7%. After annealing treatment, the tensile strength decreased to 956 MPa, while the elongation increased to 10.5%. After solid solution aging treatment, the tensile strength increased to 1020 MPa, but the elongation decreased to 8%. Therefore, for Ti-6.0Al-3.0Zr-0.5Sn-1.0Mo-1.5Nb-1.0 V alloy plates, which require high tensile strength, high yield strength and good plasticity, it is recommended to choose the annealing process: 740 °C/1 h, AC, whereas for Ti-6.0Al-3.0Zr-0.5Sn-1.0Mo-1.5Nb-1.0 V alloy plates, which require high tensile and yield strength, it is recommended to choose the solid solution aging process: 900 °C/1 h, AC. 0.5Sn-1.0Mo-1.5Nb-1.0 V alloy sheet, the solution aging process is recommended: 900 °C/0.5 h, WQ+580 °C/3 h, AC.
(3) The hot-rolled sample had obvious crystal texture, which had changed significantly after heat treatment. The hot-rolled sample exhibited strong basal texture in the {0001} pole figure. However, this texture intensity decreased after annealing at 740 °C and increased slightly after solution and aging treatment. The ODF diagram revealed that the texture type changed from Y-fiber to B-fiber due to basal slip.
(4) After annealing, the proportion of recrystallized grains in the microstructure increased to 49.98 %, and LAGBs were continuously transformed into HAGBs. The variant selection of α phase occurred after heat treatment. After solution aging treatment, stress concentration caused by dislocation accumulation and entanglement was observed at the grain boundaries. After annealing at 740 °C, the dislocations accumulation was weakened due to the increase of the proportion of recrystallized grains in the microstructure.

Acknowledgments

The work was supported by the Yunnan Provincial Major Science and Technology Special Plan of China (No. 202202AB080016) and the National Key R&D Program of China (No. 2016YFB0301202).

Data Availability

Data will be made available on request.

References

1. J. Sarma, R. Kumar, and A.K. Sahoo et al., Enhancement of Material Properties of Titanium Alloys Through Heat Treatment Process: A Brief Review, *Mater. Today Proc.*, 2020, **23**(Pt 3), p 561–564
2. Q. Zhao, Q. Sun, and S. Xin et al., High-Strength Titanium Alloys for Aerospace Engineering Applications: A Review on Melting-Forging Process, *Mater. Sci. Eng. A. Sci. Eng. A*, 2022, **845**, p 143260
3. D.Y. Pimenov, M. Mia, and M.K. Gupta et al., Improvement of Machinability of Ti and its Alloys Using Cooling-lubrication Techniques: A Review and Future Prospect, *J. Market. Res.*, 2021, **11**, p 719–753
4. G. Qiu and Y. Guo, Current Situation and Development Trend of Titanium Metal Industry in China, *Int. J. Miner. Metall. Mater.*, 2022, **29**(4), p 599–610
5. J. Fan, W. Zhang, and B. Li et al., Crystallographic Analysis of Slip System Activation in Bimodal Ti-6Al-3Nb-2Zr-1Mo Alloy Under Various Dwell-Fatigue Loadings, *Mater. Sci. Eng. A. Sci. Eng. A*, 2023, **865**, p 144610
6. B. Su, B. Wang, and L. Luo et al., Tuning Microstructure and Enhancing Corrosion Property of Ti-6Al-3Nb-2Zr-1Mo Alloy Through Electron Beam Surface Melting, *Corros. Sci.*, 2022, **206**, p 110520
7. W. Liu, S. Ao, and Y. Li et al., Effect of Anodic Behavior on Electrochemical Machining of TB6 Titanium Alloy, *Electrochim. Acta*, 2017, **233**, p 190–200
8. Z. Enrui, C. Xia, and T. Cheng et al., Simulation of Texture Evolution of TB6 Titanium Alloy Cylindrical Parts During Spinning, *Mater. Today Commun.*, 2022, **33**, p 104815
9. N.T.C. Oliveira and A.C. Guastaldi, Electrochemical Stability and Corrosion Resistance of Ti-Mo Alloys for Biomedical Applications, *Acta Biomater.*, 2009, **5**(1), p 399–405
10. D. Banerjee and J.C. Williams, Perspectives on Titanium Science and Technology, *Acta Mater.*, 2013, **61**(3), p 844–879
11. K. Meng, K. Guo, and Q. Yu et al., Effect of Annealing Temperature on the Microstructure and Corrosion Behavior of Ti-6Al-3Nb-2Zr-1Mo Alloy in Hydrochloric acid Solution, *Corros. Sci.*, 2021, **183**, p 109320
12. Z. Yang, J. Cao, and W. Yu et al., Effects of Microstructure Characteristics on the Mechanical Properties and Elastic Modulus of a New Ti-6Al-2Nb-2Zr-0.4B Alloy, *Mater. Sci. Eng. A*, 2021, **820**, p 141564
13. M.T. Tsai, Y.W. Chen, and C.Y. Chao et al., Heat-Treatment Effects on Mechanical Properties and Microstructure Evolution of Ti-6Al-4V Alloy Fabricated by Laser Powder Bed Fusion, *J. Alloys Compd.. Alloys Compd.*, 2020, **816**, p 152615
14. N. Davari, A. Rostami, and S.M. Abbasi, Effects of Annealing Temperature and Quenching Medium on Microstructure, Mechanical Properties as Well as Fatigue Behavior of Ti-6Al-4V Alloy, *Mater. Sci. Eng. A*, 2017, **683**, p 1–8
15. H.P. Ng, E. Douguet, and C.J. Bettles et al., Age-Hardening Behaviour of Two Metastable Beta-Titanium Alloys, *Mater. Sci. Eng. A*, 2010, **527**(26), p 7017–7026
16. S. Neelakantan, E.I. Galindo-Nava, and D. San Martin et al., Modelling and Design of Stress-Induced Martensite Formation in Metastable β Ti Alloys, *Mater. Sci. Eng. A*, 2014, **590**, p 140–146
17. C.L. Li, X.J. Mi, and W.J. Ye et al., A Study on the Microstructures and Tensile Properties of New Beta High Strength Titanium Alloy, *J. Alloy. Compd.*, 2013, **550**, p 23–30
18. R. Yu, Q. Chen, and P. Wang et al., Effects of Solution Temperature and Aging Time on the Microstructure and Mechanical Properties of TG6 Titanium Alloy, *J. Mater. Eng. Perform.*, 2021, **31**(2), p 1456–1464
19. P. Ding, H. Xiao, and L. Chen et al., Effect of Annealing Time on Microstructure and Mechanical Properties of Ti-6.0Al-3.0Zr-0.5Sn-1.0Mo-1.5Nb-1.0V Titanium Alloy, *Chin. J. Eng.*, 2022, **44**(01), p 50–58
20. J.W. Lu, P. Ge, and Y.Q. Zhao, Recent Development of Effect Mechanism of Alloying Elements in Titanium Alloy Design, *Rare Metal Mater. Eng.*, 2014, **43**(4), p 775–779

21. N.G. Jones, R.J. Dashwood, and M. Jackson et al., β Phase Decomposition in Ti-5Al-5Mo-5V-3Cr, *Acta Mater.*, 2009, **57**(13), p 3830–3839
22. Z. Chen, L. Xu, and Z. Liang et al., Effect of Solution Treatment and Aging on Microstructure, Tensile Properties and Creep Behavior of a Hot-Rolled β High Strength Titanium Alloy With a Composition of Ti-3.5 Al-5Mo-6V-3Cr-2Sn-0.5 Fe-01 B-0.1 C, *Mater. Scie. Eng. A*, 2021, **823**, p 141728
23. Y. Wei, Z. Pan, and Y. Fu et al., Effect of Annealing Temperatures on Microstructural Evolution and Corrosion Behavior of Ti-Mo Titanium Alloy in Hydrochloric Acid, *Corros. Sci.*, 2022, **197**, p 110079
24. X. Peng, H. Guo, and T. Wang et al., Effects of β Treatments on Microstructures and Mechanical Properties of TC4-DT Titanium Alloy, *Mater. Sci. Eng. A*, 2012, **533**, p 55–63
25. Z. Zheng, F. Kong, and X. Wang et al., The α Phase Recrystallization Mechanism and Mechanical Properties of a Near-α Titanium Matrix Composite, *Intermetallics*, 2022, **147**, p 107597
26. X. Li, X.N. Wang, and K. Liu et al., Hierarchical Structure and Deformation Behavior of a Novel Multicomponent β Titanium Alloy with Ultrahigh Strength, *J. Mater. Sci. Technol.*, 2022, **107**, p 227–242
27. G.S. Dyakonov, S. Mironov, and I.P. Semenova et al., EBSD Analysis of Grain-Refinement Mechanisms Operating During Equal-Channel Angular Pressing of Commercial-Purity Titanium, *Acta Mater.*, 2019, **173**, p 174–183
28. Y. Wang, S. Xiu, and S. Zhang, Microstructure Evolution and Crystallographic Slip Modes During Grind Hardening in TC21 Titanium Alloy, *Surf. Coat. Technol.*, 2021, **417**, p 127211
29. F. Wagner, N. Bozzolo, and O. Van Landuyt et al., Evolution of Recrystallisation Texture and Microstructure in Low Alloyed Titanium Sheets, *Acta Mater.*, 2002, **50**(5), p 1245–1259
30. H. Kamali, H.B. Xie, and F.H. Jia et al., Microstructure and Texture Evolution of Cold-Rolled Low-Ni Cr-Mn-N Austenitic Stainless Steel During Bending, *J. Mater. Sci.*, 2021, **56**(10), p 6465–6486
31. W. Chuan, Y. He, and L.H. Wei, Substructure and Texture Evolution and Flow Behavior of TA15 Titanium Alloy Compressed in the Alpha +Beta Two-Phase field, *J. Mater. Process. Technol.. Mater. Process. Technol.*, 2013, **213**(11), p 2033–2041
32. Z.B. Zhao, Q.J. Wang, and J.R. Liu et al., Characterizations of Microstructure and Crystallographic Orientation in a Near-α Titanium Alloy Billet, *J. Alloy. Compd.*, 2017, **712**, p 179–184
33. S. Balachandran, A. Kashiwar, and A. Choudhury et al., On Variant Distribution and Coarsening Behavior of the α Phase in a Metastable β Titanium Alloy, *Acta Mater.*, 2016, **106**, p 374–387
34. D. Wang, Q. Fan, and X. Cheng et al., Texture Evolution and Slip Mode of a Ti-5.5Mo-7.2Al-4.5Zr-2.6Sn-2.1Cr Dual-Phase Alloy During Cold Rolling Based on Multiscale Crystal Plasticity Finite Element Model, *J. Mater. Sci. Technol.*, 2022, **111**, p 76–87
35. S. Hu, Y.B. Tan, and W. Shi et al., Microstructure, texture evolution and mechanical behavior of Ti-3.5Al-5Mo-4V titanium alloy during hot rolling in a β field, *Mater. Today Commun.*, 2022, **31**, p 103506
36. K. Wang, M. Wu, and Z. Yan et al., Microstructure Evolution and Static Recrystallization During Hot Rolling and Annealing of an Equiaxed-Structure TC21 Titanium Alloy, *J. Alloy. Compd.*, 2018, **752**, p 14–22
37. B. Gu, P. Chekhonin, and S.W. Xin et al., Effect of Temperature and Strain Rate on the Deformation Behavior of Ti5321 During Hot-Compression, *J. Alloy. Compd.*, 2021, **876**, p 159938